e-Prime - Advances in Electrical Engineering, Electronics and Energy 5 (2023) 100200

Contents lists available at ScienceDirect

e-Prime - Advances in Electrical Engineering, Electronics and Energy

journal homepage: www.elsevier.com/locate/prime

A novel Lyapunov-based robust controller design for LCL-type shunt active power filters using adaptive sliding-mode backstepping approach

Vadood Hajbani [a], Adel Zakipour [b], Mahdi Salimi [c,*]

[a] Department of Electrical Engineering, Islamic Azad University, Ardabil Branch, Ardabil, Iran
[b] Department of Electrical Engineering, Arak University of Technology, Arak, Iran
[c] Faculty of Engineering and Science, University of Greenwich, Kent, ME4 4TB, UK

ARTICLE INFO

Keywords:
Shunt active power filter (SAPF)
LCL coupling
Hybrid control
Nonlinear control
Adaptive control
Robust control
Sliding mode control (SMC)
Uncertain parameters
Digital signal processor (DSP)

ABSTRACT

In this paper, a novel hybrid two-loop nonlinear controller is designed for stabilization and robust control of the LCL-type shunt active power filter (SAPF). To cope with the instability issue of the closed-loop system and the inherent resonance of the LCL coupling, backstepping, sliding mode and adaptive controllers are combined. DC link voltage of the grid-connected inverter is regulated in an outer control loop by determining a proper reference value for an inner loop. In addition to DC link voltage control, a major objective of the proposed closed-loop system is to make the grid current in phase with the grid voltage directly. Hence, active power filtering of the grid-connected inverter can be achieved without any current feedback from the local load. To stabilize the LCL-type SAPF in a wide range of changes, all uncertain parameters of the model including the DC link capacitor and equivalent impedances of the LCL coupling network are estimated by employing a proper Lyapunov function. For practical evaluation of the developed approach, the closed-loop system is implemented by using Texas Instruments' digital signal processor (*DSP-TMS28F335*). Considering the application of an adaptive-robust nonlinear controller, it is proved that the system enjoys a stable and robust performance over the whole range of utilization, and it doesn't suffer from resonance issues of the LCL-type SAPFs. Moreover, considering the experimental results, it is observed that the steady-state error of the proposed nonlinear controller is zero in a wide range of operations.

List of symbols and abbreviations

$\boldsymbol{X}$	vector of the system state variables
x_1, x_2, x_3 and x_4	system state variables
T	period of switching signal
D	duty cycle
u	modulation index
ρ_{1-4}	uncertain parameters
r_{L_1}	Equivalent Series Resistances (ESR) of L_1 (filter inductor)
r_{L_1}	Equivalent Series Resistances (ESR) of L_2 (filter inductor)
i_1	current of L_1 (filter inductor)
i_2	current of L_2 (filter inductor)
v_c	voltage of C (filter capacitor)
v_{dc}	voltage of C_{dc} (DC link capacitor)
i_s^*	reference value of the grid current
v_{DC}^*	reference value of DC link voltage
K_P and K_I	PI controller gains
e_{1-4}	tracking signal errors for each step
V_{1-4}	Lyapunov functions for each step
$\boldsymbol{\Gamma}$	positive diagonal matrix
S	sliding surface
$I_p, k_{1-3}, c_{1-3}, b, W$	constant value.

1. Introduction

Application of the power electronics-based and nonlinear loads e.g., battery chargers, electric motor drivers and LED lights have been increased in the recent decade to employ electric energy more efficiently. It is well-known that harmonic current can spoil the power quality of the grid at the point of common coupling (PCC), increase power losses in lines and transformers, and result in the failure of electric equipment. Hence, power quality standards and regulations are provided to determine the acceptable range of harmonic components in the electric grid. For instance, the IEEE-519 standard specifies the

* Corresponding author.
E-mail address: m.salimi@greenwich.ac.uk (M. Salimi).

https://doi.org/10.1016/j.prime.2023.100200
Received 6 December 2022; Received in revised form 24 April 2023; Accepted 16 June 2023
Available online 20 June 2023

acceptable harmonic components of the current at the PCC [1].

Traditionally, LC-type passive filters are employed widely for harmonic mitigation due to the simplicity of implementation and low cost [2]. However, the cut-off frequency passive filters cannot be tuned to adopt their characteristic during the load changes. Moreover, due to the resonance issues of passive filters, a modern generation of harmonic filters – Shunt Active Power Filters (SAPF) – is introduced. From the power topology viewpoint, SAPFs are grid-connected inverters. Since there is no active power exchange between the inverter and grid, SAPFs don't need a power source on the DC link. Regarding the requirements of AC side coupling, a passive network (L-type or LCL-type) is required as an interface between the AC terminal of the inverter and the grid [3].

The closed-loop controller of a SAPF includes three main blocks: *DC-link voltage controller, inverter output current controller and reference current calculation unit*. Inverter output reference current includes two components: an active power term to maintain the DC link voltage fixed over a defined value and inactive power [4] term for local load compensation. The active power term is determined based on the DC link voltage error. Also, inactive power is measured through analysis of the harmonic spectrum of the local load current. The stability and robustness of a SAPF can be identified based on the performance and effectiveness of the inverter output current controller and DC-link voltage controller.

From a closed-loop controller design viewpoint, SAPF is a nonlinear system due to the switching features of grid-connected inverters. Hence, the conventional linear controller cannot be assumed as a promising candidate for the implementation of the closed-loop controller required in a SAPF [5]. On the other hand, the L-type SAPF – which uses an inductor for grid coupling of the filter – has a simpler structure than LCL-type filters. State-space model of the L-type SAPF only includes two state variables: DC-link voltage and AC-side current. So, a variety of model-based modern controllers e.g., the nonlinear, adaptive, and robust have been successfully applied and tested for L-type SAPFs [6].

It should be noted that LCL-type grid-connected inverters enjoy superior performance than L-type inverters in terms of grid-current THD improvement. Considering the frequency response of an LCL, it can effectively cancel out the switching harmonics of the inverter output current and result in an almost pure sinusoidal grid current. However, from the controller viewpoint, a nonlinear closed-loop system design for LCL-type SAPF is more challenging due to model complexity and inherent resonance of the LCL network.

In [7], a dual-loop robust current controller is developed for the stabilization of an LCL-type SAPF. To extend the resonance-free region of the closed-loop system, a delay-compensation mechanism is introduced and replaced the proportional part of the conventional controllers. According to the experimental results of [7] and despite the application of an LCL-type coupling network, it is seen that the THD of the power system can only be decreased from 24.7% (local load current) to 4% (in grid current) which can be obtained using L-type inverters in a similar situation as well. Moreover, the robustness and stability of the proposed control approach aren't investigated against uncertainties of parameters.

In [8], stabilization and closed-loop control of the grid-connected inverters are investigated. Instead of implementing the active damper by using the filter capacitor feedback, a quasi-resonant controller is designed which employs the grid-side current feedback signal. So, an extra current sensor isn't needed for the implementation of an active damper. However, the controller is designed and evaluated in the Laplace domain and based on small signal approximations. Hence, the controller can only be verified around the operating point where the small-signal approximation is valid [9].

To cope with the damping issues and weak robustness of LCL-type SAPFs against grid impedance changes, the system characteristic is evaluated using open-loop pole analysis and it is shown that instability issues can arise under a large grid impedance. So, to achieve stable performance, an extra feed forward loop should be developed based on the PCC voltage. Hence, the tuning and implementation of developed control aren't straightforward.

Considering the nonlinear characteristic of LCL-type SAPFs, the application of linear controllers isn't a promising idea. Hence in [10], the combination of linear and nonlinear controllers is used for the closed-loop control of LCL-type SAPFs. A linear term of the controller is responsible for the improvement of the steady-state response and cancelling the steady-state error. On the other hand, a nonlinear term is added to the controller to improve the dynamic response. However, the stability of the controller isn't studied in a wide range of operations in [10] using nonlinear stability criteria e.g., the Lyapunov method. Also, the impact of model uncertainties and parameter changes isn't investigated.

To improve the stability and robustness of an LCL-type grid-connected inverter against grid disturbance and polytopic uncertainties of the LCL coupling filter, an adaptive current controller is developed in [11]. To achieve the full state-space control considerations without using extra measurement sensors, a discrete-time observer has been incorporated into the design. So, the closed-loop controller can lead to a low-THD grid current even in the distorted grid-voltage situation. Also, the linear quadratic approach is used for the estimation of LCL-filter uncertainties. Hence, the stability of the whole system cannot be guaranteed in a wide range of operations due to the application of a linear estimator.

To cope with the nonlinearity of LCL-type grid-connected inverters, the application of model-based nonlinear controller e.g. passivity [12], exact-feedback linearization [13], and backstepping [14] approached for the close-loop system design has attracted significant attention in recent years.

The passivity-based controller can provide proper robustness against the interferences and deal with unbalanced grid voltages. So, a three-stage cascaded passivity-based controller is designed for LCL-type grid-connected inverters in [12] to stabilize the closed-loop system in a wide range of operations. It employs three cascade controllers in a way that the first controller generates the reference signal of the second controller and similarly, the second controller provides a reference for the third one. Hence, due to the propagation delay of reference signals in the previous loops, an overall response cannot be fast enough to meet the requirements of SAPFs, e.g. for compensation of high-order harmonic components. To overcome the inherent weakness of cascade controllers, an exact feedback linearization technique is used for the controller design in LCL-type grid-connected inverters [13]. In exact feedback linearization, the nonlinear model of a system is mapped into a linear one by defining new state variables using the Lie derivatives. Suitable state variable changes can linearize the model of a nonlinear system without small-signal approximation. Hence potentially, the exact feedback linearization can stabilize a nonlinear system in a full operational range. However, in [13], the stability of the closed-loop system is analysed using the small-signal approach which isn't valid if the operating point changes widely.

Backstepping control of the LCL-type grid-connected SAPFs is a model-based controller which is designed by successive modification of the Lyapunov functions using the virtual control inputs [14]. Due to the use of the Lyapunov stability criterion, the stability and robustness of a backstepping-based controller can be maintained within the full operational range. In [14], two different controllers are designed using the backstepping approach. The first one determines the duty cycle of a DC-DC converter to ensure maximum power point operation of the photovoltaic sources. Moreover, another nonlinear controller is developed for the unity power factor operation of a multilevel grid-connected inverter. However, the impact of model parameters changes on the robustness and stability of the controller isn't studied in [14]. So, if the nominal values of the model parameters e.g., passive elements of the LCL branch, change, it can result in instability issues.

In [15], a discrete-time super-twisting adaptive sliding mode controller is developed for closed-loop control of the grid-connected

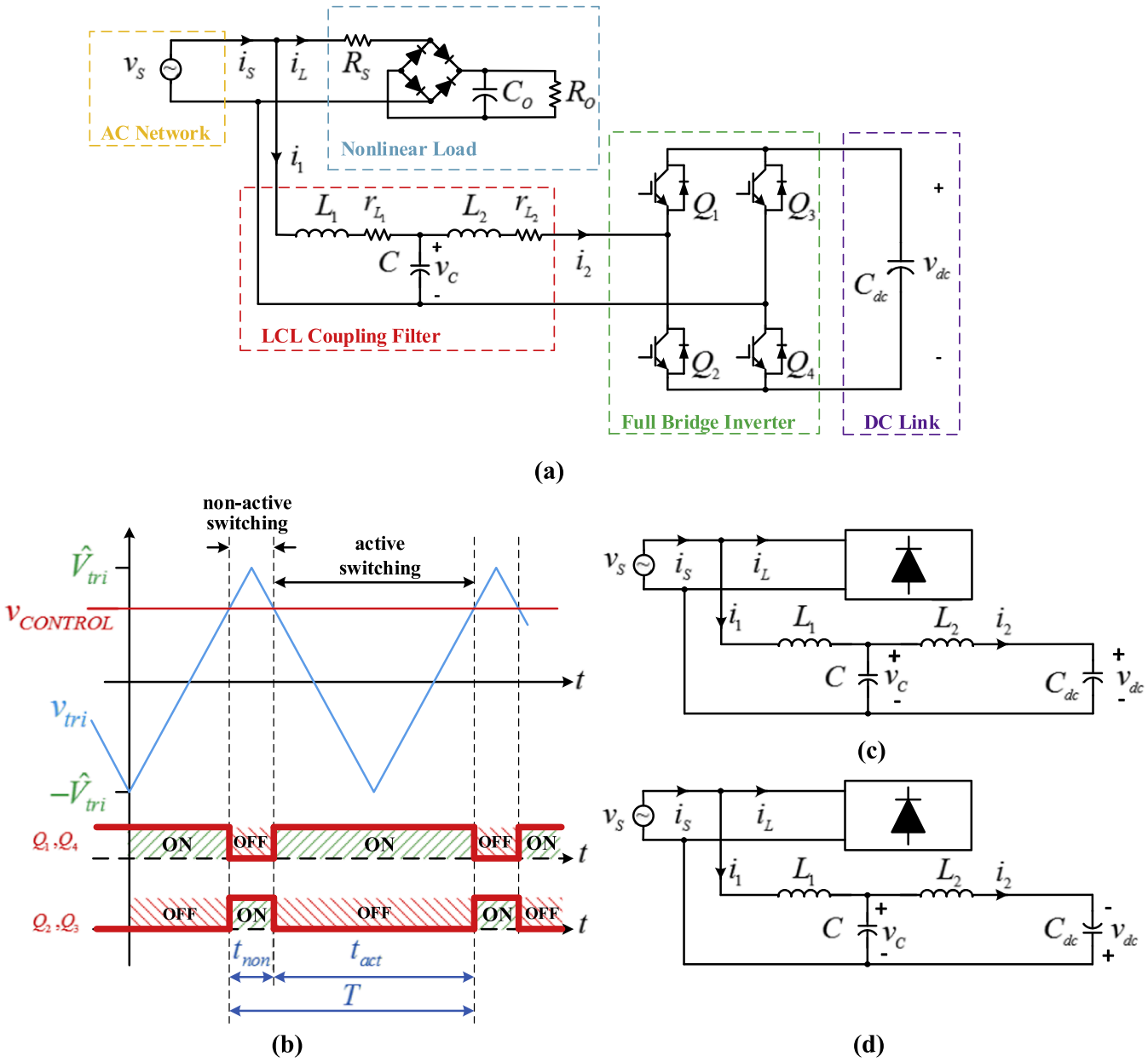

Fig. 1. (a) The circuit topology of the LCL-type SAPF in presence of a local nonlinear load (b) Bipolar SPWM switching (c) The equivalent circuit during the ON-state (active) of switching signal without ESRs and (d) OFF-state (non-active) switching interval signal without ESRs. (For interpretation of the references to color in this figure legend, the reader is referred to the web version of this article.)

inverter with LCL coupling. To investigate the robustness of the controller, a reference model is used based on the system partial model. So, the dynamics of the capacitor in the LCL coupling network are neglected to simplify the system model and obtain a first-order transfer function. Also, in [16], the one sample ahead preview approach is used for closed-loop controller design by combining the nonlinear (robust + adaptive) controllers with the predictive (deadbeat) method. The controlled plant is a three-phase grid-connected inverter with LCL coupling. Based on the adaptive feature of the designed controller, it can successfully manage the closed-loop system even in a weak grid situation. Since a three-phase inverter is studied in both [15] and [16], the multiple three harmonics of the injected currents are inherently cancelled. However, the overall THD of the proposed controllers is higher than 2.5% during the steady-state operation.

In [17], a discrete-time adaptive and robust controller is designed for grid-connected inverters with LCL coupling. The covariance matrix of the system is designed in a way that improves the controller in terms of controller dynamic response. Also, using an input-output method in [17], the closed-loop controller of the grid-connected inverter is modified to reduce the number of required sensors. The accuracy and effectiveness of the developed controller are verified using simulation and experimental results. However, the asymptotic stability and robustness of the controller aren't evaluated using the nonlinear stability criterion and hence, it cannot be guaranteed in a wide range of changes.

In [18], an observer-based sliding mode controller is developed for a grid-connected single-phase inverter with LCL coupling and its response is evaluated under weak grid circumstances. The controller estimates the state variables of the closed-loop model e.g. inverter-side inductor current and ac capacitor voltage only by measuring the grid voltage and the inverter output current. So, the number/cost of required sensors can be decreased significantly. Also, to improve the controller robustness, especially in the weak grids, an equivalent sliding mode controller is

added to the closed-loop system. However, based on the presented experimental results, it is seen that the closed-loop plant has a significant steady-state error in a wide range of changes.

In all the above references [15–18], only the output current control of the grid-connected inverter is studied and the active power functioning of the closed-loop system is not investigated. In another world, in the mentioned references, the reference current of the inverter is a pure sinusoidal current one, while in this paper, the output current of the inverter includes a wide range of high-order harmonic (depending on the local load nature) and hence, a superior dynamic response is expected from the grid-connected inverter in APF applications.

In this paper, to improve the robustness and stability of the backstepping controller against the model uncertainties, it is combined with the adaptive and robust controllers to develop a combined Lyapunov-based nonlinear controller for the closed-loop control of LCL-type SAPs. The proposed controller employs a novel hybrid two-loop nonlinear controller to cope with the instability issue of the closed-loop system and the inherent resonance of the LCL coupling. DC link voltage of the grid-connected inverter is regulated in an outer control loop by determining a proper reference value for an inner loop. In addition to DC link voltage control, the major objective of the proposed closed-loop system is to make the grid current in phase with the grid voltage directly. Hence, active power filtering of the grid-connected inverter can be achieved without any current feedback from the local load. To stabilize the LCL-type SAPF in a wide range of changes, all uncertain parameters of the model including the DC link capacitor and equivalent impedances of the LCL coupling network are estimated by employing a proper Lyapunov function. For practical evaluation of the developed approach, the closed-loop system is implemented by using Texas Instruments' digital signal processor (*DSP-TMS28F335*). Considering the application of an adaptive-robust nonlinear controller, it is proved that the system enjoys a stable and robust performance over the whole range of utilization, and it doesn't suffer from resonance issues of the LCL-type SAPFs.

2. Dynamic modelling of the LCL-type SAPF

The circuit topology of a SAPF with LCL coupling in presence of a local nonlinear load is shown in Fig. 1a. that r_{L_1} and r_{L_1} are Equivalent Series Resistances (ESR) of LCL filter Inductors.

By employing bipolar SPWM switching, the equivalent circuits of the converter during the ON (active) and OFF (non-active) states of the switching signal can be observed as shown in Fig 1. c and d, respectively. Also, in these figures the Equivalent Series Resistances (ESR) to simplify are not considered. Within the ON-state (active), Q_1 and Q_4 are ON and hence, Q_2 and Q_3 are OFF. Assuming $X = (x_1, x_2, x_3, x_4)^T = (i_1, i_2, v_c, v_{dc})^T$ as a state-space vector of the system, the state-space model of the ON-state (active) circuit in Fig. 1-c can be written as follows:

$$\dot{X} = A_1 X + B_1 \begin{bmatrix} \dot{x}_1 \\ \dot{x}_2 \\ \dot{x}_3 \\ \dot{x}_4 \end{bmatrix} = \begin{bmatrix} 0 & 0 & -1/L_1 & 0 \\ 0 & 0 & 1/L_2 & -1/L_2 \\ 1/C & -1/C & 0 & 0 \\ 0 & 1/C_{dc} & 0 & 0 \end{bmatrix} \begin{bmatrix} x_1 \\ x_2 \\ x_3 \\ x_4 \end{bmatrix} + \begin{bmatrix} v_s/L_1 \\ 0 \\ 0 \\ 0 \end{bmatrix} \tag{1}$$

Additionally, during the OFF-state (non-active) switching mode, the state space model will be (Q_1 and Q_4 are OFF while Q_2 and Q_3 are ON):

$$\dot{X} = A_2 X + B_2 \begin{bmatrix} \dot{x}_1 \\ \dot{x}_2 \\ \dot{x}_3 \\ \dot{x}_4 \end{bmatrix} = \begin{bmatrix} 0 & 0 & -1/L_1 & 0 \\ 0 & 0 & 1/L_2 & 1/L_2 \\ 1/C & -1/C & 0 & 0 \\ 0 & -1/C_{dc} & 0 & 0 \end{bmatrix} \begin{bmatrix} x_1 \\ x_2 \\ x_3 \\ x_4 \end{bmatrix} + \begin{bmatrix} v_s/L_1 \\ 0 \\ 0 \\ 0 \end{bmatrix} \tag{2}$$

It is well-known that these equations can be merged using the state-space averaging technique. So, the system's model can be written as $\dot{X} = A_{avg} X + B_{avg}$ in which $A_{avg} = (1/T)(t_{act} A_{act} + t_{non} A_{non})$ and $B_{avg} = (1/T)(t_{act} B_{act} + t_{non} B_{non})$ are the average values of state-space matrices. By definition, $t_{act} = DT$ and $t_{non} = (1-D)T$ where $D \in [0,1]$ is the switching signal duty cycle. As a result, the average value of the state space variables is written in (3)

$$A_{avg} = \begin{bmatrix} 0 & 0 & -1/L_1 & 0 \\ 0 & 0 & 1/L_2 & -(2D-1)/L_2 \\ 1/C & -1/C & 0 & 0 \\ 0 & (2D-1)/C_{dc} & 0 & 0 \end{bmatrix}, \quad B_{avg} = \begin{bmatrix} v_s/L_1 \\ 0 \\ 0 \\ 0 \end{bmatrix} \tag{3}$$

Considering the bipolar SPWM switching, the inverter modulation index (u) can be defined as $u = 2D - 1$, where $u \in [-1, 1]$ [19]. Assuming the inverter modulation index as a control variable, the averaged state-space model can be rewritten as:

$$\begin{bmatrix} \dot{x}_1 \\ \dot{x}_2 \\ \dot{x}_3 \\ \dot{x}_4 \end{bmatrix} = \begin{bmatrix} 0 & 0 & -\rho_1 & 0 \\ 0 & 0 & \rho_2 & -u\rho_2 \\ \rho_3 & -\rho_3 & 0 & 0 \\ 0 & u\rho_4 & 0 & 0 \end{bmatrix} \begin{bmatrix} x_1 \\ x_2 \\ x_3 \\ x_4 \end{bmatrix} + \begin{bmatrix} \rho_1 v_s \\ 0 \\ 0 \\ 0 \end{bmatrix} \tag{4}$$

In which $\rho_1 = \frac{1}{L_1}$, $\rho_2 = \frac{1}{L_2}$, $\rho_3 = \frac{1}{C}$, and $\rho_4 = \frac{1}{C_{dc}}$ are uncertain parameters.

3. Controller design

For local load compensation, the grid-connected inverter should generate a well-defined current waveform (reference current of the controller) which includes all harmonic and reactive components of the local load current. Considering the overall structure of the proposed controller in Fig. 2, the inner loop which is responsible for output-current control will be implemented by using the proposed hybrid nonlinear control approach.

As explained, inverter reference current includes reactive and all high-frequency harmonic components of load current. If the SAPF generates the mentioned reference current, it will result in a pure sinusoidal grid current which is in phase with the grid voltage. So, it can be concluded that the grid reference current should be a pure sinusoidal waveform and in phase with the grid voltage. In this paper, to facilitate the reference current calculation process, the grid current controller is employed rather than a current controller for SAPF. The magnitude of the grid reference current will be determined based on the DC link voltage error.

Briefly, if the DC link voltage of a SAPF is stabilized at a constant value (due to the lack of an independent voltage source on the DC side) and if a sinusoidal active current is defined as a grid reference based on the DC link voltage error, it can be concluded that the total reactive and harmonic power of the local load is supplied by the SAPF.

3.1. Outer controller – Voltage loop design

In the proposed controller, a proportional-integral (PI) controller is used in the outer voltage loop. If the load compensation is achieved, a sinusoidal current will be delivered through the grid which is in phase with the grid voltage. Consequently, the grid reference current can be represented as follows

$$i_s^* = I_p \sin\theta \tag{5}$$

In this equation, i_s^* demonstrates the reference value of the grid current and also I_p is a constant value. The value of I_p depends on the characteristic of the local load and is determined by the outer loop in Fig. 2, based on the DC link voltage error. In this figure, $(\sin\theta)$ will be generated by a phase-locked loop (PLL) circuit. To track the reference current in the inner loop, a hybrid adaptive robust backstepping is developed to control the filter output current.

The external loop generates the grid reference current (i_s^*) and subsequently, the filter reference current $(i_1^* = x_1^*)$. In this situation, the DC link voltage will be equal to its reference value (v_{DC}^*). According to Fig. 2,

the PI controller is defined as follows

$$I_p = \left(K_P + \frac{K_I}{s}\right)\left(v_{DC}^* - v_{DC}\right) = \left(K_P + \frac{K_I}{s}\right)e_V \tag{6}$$

where the PI controller gains are K_P and K_I.

3.2. Internal controller – Current loop design

This controller adjusts the switching signal of the inverter (u) to control the filter output current. As explained, the reference value of the inverter current is $i_1^* = i_s^* - i_L$. In this situation, all the reactive and harmonic components of nonlinear local loads will be provided through the SAPF. Considering the nonlinear characteristic of SAPF, in this paper, a nonlinear hybrid controller is developed for the internal loop. Also, it is assumed that all model parameters are uncertain, and the controller should estimate the uncertainties using an appropriate estimation rule.

The step-by-step procedure for adaptive-sliding-backstepping controller design can be summarised as follows:

1 State-space modelling of the plant.
2 Defining the reference value of the state variables considering the overall purpose of the closed-loop system
3 Defining the actual error variables
4 Defining the virtual error variables based on the stability criteria
5 Defining the sliding surface as a linear combination of all error variables including actual and virtual errors
6 Updating the stability criteria by adding the square of the sliding surface to the Lyapunov function

Below, the controller design detail is presented which includes four steps.

Step 1: The tracking signal error is defined as follows

$$e_1 = x_1 - x_1^* \tag{7}$$

where x_1^* is the reference value of x_1 determined by the external loop based on the voltage error of the DC link. So

$$\dot{e}_1 = \dot{x}_1 - \dot{x}_1^* \tag{8}$$

By substituting $\dot{x}_1$ from (4) in (8), it can be rewritten as

$$\dot{e}_1 = \widehat{\boldsymbol{P}}^T\boldsymbol{M}_1 - \dot{x}_1^* + (\boldsymbol{P} - \widehat{\boldsymbol{P}})^T\boldsymbol{M}_1 \tag{9}$$

where

$$\widehat{\boldsymbol{P}}^T = [\,\widehat{\rho}_1 \quad \widehat{\rho}_2 \quad \widehat{\rho}_3 \quad \widehat{\rho}_4\,] \tag{10}$$

$$\boldsymbol{M}_1 = [\,-x_3 + v_s \quad 0 \quad 0 \quad 0\,]^T \tag{11}$$

The Lyapunov function of the system can be selected as follows:

$$V_1 = 0.5e_1^2 + (\boldsymbol{P} - \widehat{\boldsymbol{P}})^T\boldsymbol{\Gamma}^{-1}(\boldsymbol{P} - \widehat{\boldsymbol{P}}) \tag{12}$$

In this equation, $\boldsymbol{\Gamma}$ is a positive diagonal matrix and its diagonal arrays are called estimated particle weights. The derivative of V_1 can be written as

$$\dot{V}_1 = e_1\dot{e}_1 + (\boldsymbol{P} - \widehat{\boldsymbol{P}})^T\boldsymbol{\Gamma}^{-1}(-\dot{\widehat{\boldsymbol{P}}}) \tag{13}$$

By substituting (9) in (13) $\dot{V}_1$ can be rewritten

$$\dot{V}_1 = e_1\left(\widehat{\boldsymbol{P}}^T\boldsymbol{M}_1 - \dot{x}_1^*\right) + (\boldsymbol{P} - \widehat{\boldsymbol{P}})^T\boldsymbol{\Gamma}^{-1}\left(-\dot{\widehat{\boldsymbol{P}}} + \boldsymbol{\Gamma}e_1\boldsymbol{M}_1\right) \tag{14}$$

If $\widehat{\boldsymbol{P}}^T\boldsymbol{M}_1 - \dot{x}_1^* = -k_1e_1$ and $--\dot{\widehat{\boldsymbol{P}}} + \boldsymbol{\Gamma}e_1\boldsymbol{M}_1 = 0$ are considered in (14), then (14) will be simplified like $\dot{V}_1 = -k_1e_1^2 \le 0$, which is a semi-definite negative function and guarantees the asymptotic stability of the system. In these equations, $k_1 \ge 0$ is a constant scalar value.

Step 2: Given that $(--k_1e_1)$ and $(\widehat{\boldsymbol{P}}^T\boldsymbol{M}_1 - \dot{x}_1^*)$ are not necessarily equal, the error of these two variables is defined as the second error variable:

$$e_2 = -k_1e_1 - \left[\widehat{\boldsymbol{P}}^T\boldsymbol{M}_1 - \dot{x}_1^*\right] \tag{15}$$

By substituting (15) in (9):

$$\dot{e}_1 = -k_1e_1 - e_2 + (\boldsymbol{P} - \widehat{\boldsymbol{P}})^T\boldsymbol{M}_1 \tag{16}$$

The derivative of e_2 will be equal to

$$\dot{e}_2 = \dot{\widehat{\rho}}_1x_3 + \widehat{\rho}_1\dot{x}_3 - \dot{\widehat{\rho}}_1v_s - \widehat{\rho}_1\dot{v}_s + \ddot{x}_1^* - c_1\dot{e}_1 \tag{17}$$

By taking $\widehat{\boldsymbol{P}}$ and $\boldsymbol{M}_1$ into account from (10) and (11), the time derivative is simplified as follows

$$\dot{e}_2 = A + \widehat{\boldsymbol{P}}^T\boldsymbol{M}_2 + (\boldsymbol{P} - \widehat{\boldsymbol{P}})^T(-k_1\boldsymbol{M}_1 + \boldsymbol{M}_2) \tag{18}$$

which

$$A = \dot{\widehat{\rho}}_1x_3 - \dot{\widehat{\rho}}_1v_s - \widehat{\rho}_1\dot{v}_s + \ddot{x}_1^* + k_1^2e_1 + k_1e_2 \tag{19}$$

$$\boldsymbol{M}_2^T = [\,0 \quad 0 \quad \widehat{\rho}_1x_1 - \widehat{\rho}_1x_2 \quad 0\,] \tag{20}$$

Similarly, by updating the Lyapunov function as

$$V_2 = 0.5e_1^2 + 0.5e_2^2 + (\boldsymbol{P} - \widehat{\boldsymbol{P}})^T\boldsymbol{\Gamma}^{-1}(\boldsymbol{P} - \widehat{\boldsymbol{P}}) \tag{21}$$

its derivative can be simplified

$$\begin{aligned}\dot{V}_2 = &-k_1e_1^2 + e_2\left[-e_1 + A + \widehat{\boldsymbol{P}}^T\boldsymbol{M}_2\right] \\ &+ (\boldsymbol{P} - \widehat{\boldsymbol{P}})^T\boldsymbol{\Gamma}^{-1}\left(-\dot{\widehat{\boldsymbol{P}}} + \boldsymbol{\Gamma}e_1\boldsymbol{M}_1 - k_1\boldsymbol{\Gamma}e_2\boldsymbol{M}_1 + \boldsymbol{\Gamma}e_2\boldsymbol{M}_2\right)\end{aligned} \tag{22}$$

If, in (22), it is considered that $-e_1 + A + \widehat{\boldsymbol{P}}^T\boldsymbol{M}_2 = -k_2e_2$ and $-\dot{\widehat{\boldsymbol{P}}} + \boldsymbol{\Gamma}e_1\boldsymbol{M}_1 - e_1\boldsymbol{\Gamma}e_2\boldsymbol{M}_1 + \boldsymbol{\Gamma}e_2\boldsymbol{M}_2 = 0$, in this case, (22) will be simplified as $\dot{V}_2 = -k_1e_1^2 - k_2e_2^2$ and will guarantee the asymptotic stability of the system. In these equations, $k_2 \ge 0$ is a constant scalar value.

Step 3: Similarity, as $(--k_2e_2)$ and $(--e_1 + A + \widehat{\boldsymbol{P}}^T\boldsymbol{M}_2)$ are not necessarily equal, the error of these two variables is defined as the third error variable

$$e_3 = -k_2e_2 - \left(-e_1 + A + \widehat{\boldsymbol{P}}^T\boldsymbol{M}_2\right) \tag{23}$$

By substituting (23) in (18)

$$\dot{e}_2 = e_1 - k_2e_2 - e_3 + (\boldsymbol{P} - \widehat{\boldsymbol{P}})^T(-k_1\boldsymbol{M}_1 + \boldsymbol{M}_2) \tag{24}$$

The time derivative of e_3 will be like

$$\begin{aligned}\dot{e}_3 = &\left(1 - k_1^2\right)\dot{e}_1 - (k_1 + k_2)\dot{e}_2 - (\dot{\widehat{\rho}}_1\widehat{\rho}_3 + \widehat{\rho}_1\dot{\widehat{\rho}}_3)x_1 - \widehat{\rho}_1\widehat{\rho}_3\dot{x}_1 + (\dot{\widehat{\rho}}_1\widehat{\rho}_3 \\ &+ \widehat{\rho}_1\dot{\widehat{\rho}}_3)x_2 + \widehat{\rho}_1\widehat{\rho}_3\dot{x}_2 - \ddot{\widehat{\rho}}_1x_3 - \dot{\widehat{\rho}}_1\dot{x}_3 + \ddot{\widehat{\rho}}_1v_s + 2\dot{\widehat{\rho}}_1\dot{v}_s + \widehat{\rho}_1\ddot{v}_s - \dddot{x}_1^*\end{aligned} \tag{25}$$

By taking $\widehat{\boldsymbol{P}}$, $\boldsymbol{M}_1$ and $\boldsymbol{M}_2$ into account from (10), (11) and (20), the time derivative can be simplified as

$$\dot{e}_3 = B + \widehat{\boldsymbol{P}}^T\boldsymbol{M}_3 + (\boldsymbol{P} - \widehat{\boldsymbol{P}})^T[(k_1k_2 + 1)\boldsymbol{M}_1 - (k_1 + k_2)\boldsymbol{M}_2 + \boldsymbol{M}_3] \tag{26}$$

Which

$$\begin{aligned}B = &\left(-2k_1 + k_1^3 - k_2\right)e_1 + \left(-1 + k_1^2 + k_1k_2 + k_2^2\right)e_2 + (k_1 + k_2)e_3 \\ &- (\dot{\widehat{\rho}}_1\widehat{\rho}_3 + \widehat{\rho}_1\dot{\widehat{\rho}}_3)x_1 + (\dot{\widehat{\rho}}_1\widehat{\rho}_3 + \widehat{\rho}_1\dot{\widehat{\rho}}_3)x_2 - \ddot{\widehat{\rho}}_1x_3 + \ddot{\widehat{\rho}}_1v_s + 2\dot{\widehat{\rho}}_1\dot{v}_s + \widehat{\rho}_1\ddot{v}_s - \dddot{x}_1^*\end{aligned} \tag{27}$$

$$\boldsymbol{M}_3 = \begin{bmatrix} +\widehat{\rho}_1\widehat{\rho}_3x_3 - \widehat{\rho}_1\widehat{\rho}_3v_s \\ +\widehat{\rho}_1\widehat{\rho}_3x_3 - u\widehat{\rho}_1\widehat{\rho}_3x_4\,x_1 + \dot{\widehat{\rho}}_1x_20 \\ -\dot{\widehat{\rho}}_1 \end{bmatrix} \tag{28}$$

Similarly, by choosing the Lyapunov function as

$$V_3 = 0.5e_1^2 + 0.5e_2^2 + 0.5e_3^2 + (\boldsymbol{P} - \widehat{\boldsymbol{P}})^T \boldsymbol{\Gamma}^{-1} (\boldsymbol{P} - \widehat{\boldsymbol{P}}) \tag{29}$$

its derivative can be simplified like

$$\dot{V}_3 = -k_1 e_1^2 - k_2 e_2^2 + e_3\big[- e_2 + B + \widehat{\boldsymbol{P}}^T \boldsymbol{M}_3\big] + (\boldsymbol{P} - \widehat{\boldsymbol{P}})^T \boldsymbol{\Gamma}^{-1}\{ - \dot{\widehat{\boldsymbol{P}}} + \boldsymbol{\Gamma}[(e_1 - k_1 e_2 + (k_1 k_2 + 1)e_3)\boldsymbol{M}_1 + (e_2 - (k_1 + k_2)e_3)\boldsymbol{M}_2 + e_3 \boldsymbol{M}_3]\} \tag{30}$$

If in (30) it is assumed that $- e_2 + B + \widehat{\boldsymbol{P}}^T \boldsymbol{M}_3 = - k_3 e_3$ and $- \dot{\widehat{\boldsymbol{P}}} + \boldsymbol{\Gamma} e_1 \boldsymbol{M}_1 - k_1 \boldsymbol{\Gamma} e_2 \boldsymbol{M}_1 + \boldsymbol{\Gamma} e_2 \boldsymbol{M}_2 + (k_1 k_2 + 1)\boldsymbol{\Gamma} e_3 \boldsymbol{M}_1 - (k_1 + k_2)\boldsymbol{\Gamma} e_3 \boldsymbol{M}_2 + \boldsymbol{\Gamma} e_3 \boldsymbol{M}_3 = 0$, then the (22) will be simplified like $\dot{V}_3 = -k_1 e_1^2 - k_2 e_2^2 - k_3 e_3^2$ that ensures the asymptotic stability of the system. In these equations, k_3 the constant scalar value is positive.

Step 4: Finally, as $(- - k_3 e_3)$ and $(- - e_2 + B + \widehat{\boldsymbol{P}}^T \boldsymbol{M}_3)$ are not equal, the error of these two variables will be defined as the fourth error variable

$$e_4 = -k_3 e_3 - \big(- e_2 + B + \widehat{\boldsymbol{P}}^T \boldsymbol{M}_3\big) \tag{31}$$

By substituting (31) in (23) the following equation can be written

$$\dot{e}_3 = e_2 - k_3 e_3 - e_4 + (\boldsymbol{P} - \widehat{\boldsymbol{P}})^T [(k_1 k_2 + 1)\boldsymbol{M}_1 - (k_1 + k_2)\boldsymbol{M}_2 + \boldsymbol{M}_3] \tag{32}$$

Considering (10) and (28), the e_4 time derivative will be simplified as

$$\dot{e}_4 = C + \widehat{\boldsymbol{P}}^T \boldsymbol{M}_4 + (\boldsymbol{P} - \widehat{\boldsymbol{P}})^T [(- k_1 - k_1 k_2 k_3 - k_3)\boldsymbol{M}_1 + (+ k_1 k_2 + k_1 k_3 + k_2 k_3 + 2)\boldsymbol{M}_2 - q_{c4}\boldsymbol{M}_3 + \boldsymbol{M}_4] \tag{33}$$

which

$$S = c_1 e_1 + c_2 e_2 + c_3 e_3 + e_4 \tag{38}$$

In these equations, c_1, c_2, and c_3 are constant scalar values. The time derivative of Lyapunov function $(\dot{V}_4)$ can be determined as

$$\dot{V}_4 = e_1 \dot{e}_1 + e_2 \dot{e}_2 + e_3 \dot{e}_3 + S\dot{S} + (\boldsymbol{P} - \widehat{\boldsymbol{P}})^T \boldsymbol{\Gamma}^{-1} (-\dot{\widehat{\boldsymbol{P}}}) \tag{39}$$

or

$$\dot{V}_4 = q_{v11} e_1^2 + q_{v12} e_1 e_2 + q_{v13} e_1 e_3 + q_{v14} e_1 e_4 + q_{v22} e_2^2 + q_{v23} e_2 e_3 + q_{v24} e_2 e_4 + q_{v33} e_3^2 + q_{v34} e_3 e_4 - c_3 e_4^2 + (c_1 e_1 + c_2 e_2 + c_3 e_3 + e_4) C + (\boldsymbol{P} - \widehat{\boldsymbol{P}})^T \boldsymbol{\Gamma}^{-1}\{ - \dot{\widehat{\boldsymbol{P}}} + \boldsymbol{\Gamma}[(e_1 - k_1 e_2 + k_1 k_2 e_3 + e_3)\boldsymbol{M}_1 + (+ e_2 - k_1 e_3 - k_2 e_3)\boldsymbol{M}_2 + e_3 \boldsymbol{M}_3 + (c_1 e_1 + c_2 e_2 + c_3 e_3 + e_4)(q_{v1}\boldsymbol{M}_1 + q_{v2}\boldsymbol{M}_2 + q_{v3}\boldsymbol{M}_3 + \boldsymbol{M}_4)]\} \tag{40}$$

Which

$$\begin{aligned} q_{v11} &= -k_1 - k_1 c_1^2 + c_1 c_2 \; q_{v12} = -k_1 c_1 c_2 - k_2 c_1 c_2 - c_1^2 + c_2^2 + c_1 c_3 \; q_{v13} \\ &= -k_1 c_1 c_3 - k_3 c_1 c_3 - c_1 c_2 + c_2 c_3 \; q_{v14} = -k_1 c_1 + c_2 - c_1 c_3 \; q_{v22} \\ &= -k_2 - k_2 c_2^2 - c_1 c_2 + c_2 c_3 \; q_{v23} = -k_2 c_2 c_3 - k_3 c_2 c_3 - c_2^2 c_3^2 - c_1 c_3 \; q_{v24} \\ &= -k_2 c_2 - c_1 + c_3 - c_2 c_3 \; q_{v33} = -k_3 - k_3 c_3^2 - c_2 c_3 \; q_{v34} \\ &= -1 - k_3 c_3 - c_2 - c_3^2 \; q_{v1} \\ &= -k_1 - k_1 k_2 k_3 - k_3 + c_1 - k_1 c_2 + k_1 k_2 c_3 + c_3 \; q_{v2} \\ &= +2 + k_1 k_2 + k_1 k_3 + k_2 k_3 + c_2 - k_1 c_3 - k_2 c_3 \; q_{v3} = -k_1 - k_2 - k_3 + c_3 \end{aligned} \tag{41}$$

If in the previous equation, it is assumed that

$$\begin{aligned} C = {} & q_{c1} e_1 + q_{c2} e_2 + q_{c3} e_3 + q_{c4} e_4 + \big(3\dot{\hat{\rho}}_1 \dot{\hat{\rho}}_3 + \hat{\rho}_1 \ddot{\hat{\rho}}_3\big) x_1 \\ & + \big(2\ddot{\hat{\rho}}_1 \hat{\rho}_3 - 2\ddot{\hat{\rho}}_1 \hat{\rho}_3 - 3\dot{\hat{\rho}}_1 \dot{\hat{\rho}}_3 - \hat{\rho}_1 \ddot{\hat{\rho}}_3\big) x_2 \\ & + \big(\dddot{\hat{\rho}}_1 - \hat{\rho}_1 \dot{\hat{\rho}}_2 \hat{\rho}_3 - \hat{\rho}_1^2 \dot{\hat{\rho}}_3 - \dot{\hat{\rho}}_1 \hat{\rho}_2 \hat{\rho}_3 - \hat{\rho}_1 \dot{\hat{\rho}}_2 \hat{\rho}_3 - \hat{\rho}_1 \hat{\rho}_2 \dot{\hat{\rho}}_3\big) x_3 \\ & + \big(\dot{u}\hat{\rho}_1 \hat{\rho}_2 \hat{\rho}_3 + u\dot{\hat{\rho}}_1 \hat{\rho}_2 \hat{\rho}_3 + u\hat{\rho}_1 \dot{\hat{\rho}}_2 \hat{\rho}_3 + u\hat{\rho}_1 \hat{\rho}_2 \dot{\hat{\rho}}_3\big) x_4 \\ & + \big(\hat{\rho}_1 \dot{\hat{\rho}}_1 \hat{\rho}_3 + \hat{\rho}_1^2 \dot{\hat{\rho}}_3 - \dddot{\hat{\rho}}_1\big) v_s + \big(\hat{\rho}_1^2 \hat{\rho}_3 - 3\ddot{\hat{\rho}}_1\big)\dot{v}_s - 3\dot{\hat{\rho}}_1 \ddot{v}_s - \hat{\rho}_1 \dddot{v}_s + \dddot{x}_1^* \end{aligned} \tag{34}$$

$$\boldsymbol{M}_4 = \begin{bmatrix} (- \hat{\rho}_1 \dot{\hat{\rho}}_3 - 2\dot{\hat{\rho}}_1 \hat{\rho}_3) x_3 + (\hat{\rho}_1 \dot{\hat{\rho}}_3 + 2\dot{\hat{\rho}}_1 \hat{\rho}_3) v_s \\ (- \hat{\rho}_1 \dot{\hat{\rho}}_3 - 2\dot{\hat{\rho}}_1 \hat{\rho}_3) x_3 + (u\hat{\rho}_1 \dot{\hat{\rho}}_3 + 2u\dot{\hat{\rho}}_1 \hat{\rho}_3) x_4 \\ \big(- \hat{\rho}_1 \hat{\rho}_2 \hat{\rho}_3 - \hat{\rho}_1^2 \hat{\rho}_3 + \ddot{\hat{\rho}}_1\big) x_1 + \big(\hat{\rho}_1 \hat{\rho}_2 \hat{\rho}_3 - \ddot{\hat{\rho}}_1 + \hat{\rho}_1^2 \hat{\rho}_3\big) x_2 \\ + u^2 \hat{\rho}_1 \hat{\rho}_2 \hat{\rho}_3 x_2 \end{bmatrix} \tag{35}$$

$$\begin{aligned} q_{c1} &= k_1^4 - 3k_1^2 - 2k_1 k_2 - k_2^2 + 2 \; q_{c2} \\ &= k_1^3 - 3k_1 + k_1^2 k_2 + k_1 k_2^2 - 4k_2 + k_2^3 - k_3 \; q_{c3} \\ &= k_1^2 + k_1 k_2 + k_2^2 + k_1 k_3 + k_2 k_3 + k_3^2 - 2 \; q_{c4} = k_1 + k_2 + k_3 \end{aligned} \tag{36}$$

By updating of the Lyapunov function as:

$$V_4 = 0.5e_1^2 + 0.5e_2^2 + 0.5e_3^2 + 0.5S^2 + (\boldsymbol{P} - \widehat{\boldsymbol{P}})^T \boldsymbol{\Gamma}^{-1} (\boldsymbol{P} - \widehat{\boldsymbol{P}}) \tag{37}$$

where S represents the sliding surface of the controller and is defined as

$$C + \widehat{\boldsymbol{P}}^T \boldsymbol{M}_4 = -b(S + Wsgn(S)) \tag{42}$$

and

$$-\dot{\widehat{\boldsymbol{P}}} + \boldsymbol{\Gamma}[(e_1 - k_1 e_2 + k_1 k_2 e_3 + e_3)\boldsymbol{M}_1 + (+ e_2 - k_1 e_3 - k_2 e_3)\boldsymbol{M}_2 + e_3 \boldsymbol{M}_3 + (c_1 e_1 + c_2 e_2 + c_3 e_3 + e_4)(q_{v1}\boldsymbol{M}_1 + q_{v2}\boldsymbol{M}_2 + q_{v3}\boldsymbol{M}_3 + \boldsymbol{M}_4)] = 0 \tag{43}$$

Then Eq. (39) can be simplified as (42) if Eq. (43) is satisfied.

$$\dot{V}_4 = q_{v11} e_1^2 + q_{v12} e_1 e_2 + q_{v13} e_1 e_3 + q_{v14} e_1 e_4 + q_{v22} e_2^2 + q_{v23} e_2 e_3 + q_{v24} e_2 e_4 + q_{v33} e_3^2 + q_{v34} e_3 e_4 - c_3 e_4^2 - bS^2 - bW|S| \tag{44}$$

$$\sqrt{q_{v11} q_{v22}} = -\frac{1}{2} q_{v12} \;\; \sqrt{q_{v11} q_{v33}} = -\frac{1}{2} q_{v13} \;\; \sqrt{-c_3 q_{v11}} = -\frac{1}{2} q_{v14} \tag{45}$$

By using Eqs. (42) and (43), adaptive nonlinear controller (u) and uncertain parameters estimation rules ($\hat{\rho}_i$ for $i = 1 - 4$) are achieved by

$$
\begin{aligned}
&(+\hat{\rho}_1\hat{\rho}_2\hat{\rho}_3)x_4\dot{u} + (\hat{\rho}_1\hat{\rho}_2\hat{\rho}_3\hat{\rho}_4)x_2u^2 + \left(+3\dot{\hat{\rho}}_1\hat{\rho}_2\hat{\rho}_3 + \hat{\rho}_1\dot{\hat{\rho}}_2\hat{\rho}_3 + 2\hat{\rho}_1\hat{\rho}_2\dot{\hat{\rho}}_3\right)x_4u \\
&\quad = -q_{c1}e_1 - q_{c2}e_2 - q_{c3}e_3 - q_{c4}e_4 \\
&\quad + \left(+\hat{\rho}_1\hat{\rho}_2\hat{\rho}_3^2 + \hat{\rho}_1^2\hat{\rho}_3^2 - \ddot{\hat{\rho}}_1 - 3\dot{\hat{\rho}}_1\dot{\hat{\rho}}_3 - \hat{\rho}_1\ddot{\hat{\rho}}_3\right)x_1 \\
&\quad + \left(+3\dot{\hat{\rho}}_1\dot{\hat{\rho}}_3 + \hat{\rho}_1\ddot{\hat{\rho}}_3 - \hat{\rho}_1\hat{\rho}_2\hat{\rho}_3^2 + \ddot{\hat{\rho}}_1\hat{\rho}_3 - \hat{\rho}_1^2\hat{\rho}_3^2\right)x_2 \\
&\quad + \left(+3\dot{\hat{\rho}}_1\hat{\rho}_2\hat{\rho}_3 + 2\hat{\rho}_1\dot{\hat{\rho}}_2\hat{\rho}_3 + 2\hat{\rho}_1\hat{\rho}_2\dot{\hat{\rho}}_3 - \dddot{\hat{\rho}}_1 + 2\hat{\rho}_1^2\dot{\hat{\rho}}_3 + 2\hat{\rho}_1\dot{\hat{\rho}}_1\hat{\rho}_3\right)x_3 \\
&\quad + \left(+\dddot{\hat{\rho}}_1 - 2\hat{\rho}_1^2\dot{\hat{\rho}}_3 - 3\hat{\rho}_1\dot{\hat{\rho}}_1\hat{\rho}_3\right)v_s + \left(-\hat{\rho}_1^2\hat{\rho}_3 + 3\ddot{\hat{\rho}}_1\right)\dot{v}_s + 3\dot{\hat{\rho}}_1\ddot{v}_s + \hat{\rho}_1\dddot{v}_s - \dddot{x}_1^* \\
&\quad - b\left(S + Wsgn(S)\right)
\end{aligned}
\tag{46}
$$

and

$$
\begin{aligned}
\dot{\hat{\rho}}_1 &= \gamma_{11}\{[(e_1 - k_1e_2 + k_1k_2e_3 + e_3) + q_{v1}(c_1e_1 + c_2e_2 + c_3e_3 + e_4)](-x_3 + v_s) \\
&\quad + [e_3 + q_{v3}(c_1e_1 + c_2e_2 + c_3e_3 + e_4)](+\hat{\rho}_1\hat{\rho}_3x_3 - \hat{\rho}_1\hat{\rho}_3v_s) \\
&\quad + (c_1e_1 + c_2e_2 + c_3e_3 + e_4)(-\hat{\rho}_1\hat{\rho}_3x_3 + \hat{\rho}_1\hat{\rho}_3v_s - 2\dot{\hat{\rho}}_1\hat{\rho}_3x_3 + 2\dot{\hat{\rho}}_1\hat{\rho}_3v_s)\}
\end{aligned}
\tag{47}
$$

$$
\begin{aligned}
\dot{\hat{\rho}}_2 &= \gamma_{22}\{[e_3 + q_{v3}(c_1e_1 + c_2e_2 + c_3e_3 + e_4)](+\hat{\rho}_1\hat{\rho}_3x_3 - u\hat{\rho}_1\hat{\rho}_3x_4) \\
&\quad + (c_1e_1 + c_2e_2 + c_3e_3 + e_4)(-\hat{\rho}_1\dot{\hat{\rho}}_3x_3 - 2\dot{\hat{\rho}}_1\hat{\rho}_3x_3 + u\hat{\rho}_1\dot{\hat{\rho}}_3x_4 + 2u\dot{\hat{\rho}}_1\hat{\rho}_3x_4)\}
\end{aligned}
\tag{48}
$$

$$
\begin{aligned}
\dot{\hat{\rho}}_3 &= \gamma_{33}\Big\{[(+e_2 - k_1e_3 - k_2e_3) + q_{v2}(c_1e_1 + c_2e_2 + c_3e_3 + e_4)](\hat{\rho}_1x_1 - \hat{\rho}_1x_2) \\
&\quad + [e_3 + q_{v3}(c_1e_1 + c_2e_2 + c_3e_3 + e_4)](-\dot{\hat{\rho}}_1x_1 + \dot{\hat{\rho}}_1x_2) \\
&\quad + (c_1e_1 + c_2e_2 + c_3e_3 + e_4)\Big(-\hat{\rho}_1\hat{\rho}_2\hat{\rho}_3x_1 - \hat{\rho}_1^2\hat{\rho}_3x_1 + \ddot{\hat{\rho}}_1x_1 \\
&\quad + \hat{\rho}_1\hat{\rho}_2\hat{\rho}_3x_2 - \ddot{\hat{\rho}}_1x_2 + \hat{\rho}_1^2\hat{\rho}_3x_2\Big)\Big\}
\end{aligned}
\tag{49}
$$

$$
\dot{\hat{\rho}}_4 = \gamma_{44}\{(c_1e_1 + c_2e_2 + c_3e_3 + e_4)(+u^2\hat{\rho}_1\hat{\rho}_2\hat{\rho}_3x_2)\}
\tag{50}
$$

4. Practical results

To examine the response of the developed adaptive-nonlinear controller, the SAPF with LCL coupling is implemented practically, and the experiment results are presented in this section. The controller and the uncertain parameters estimation rules are extracted in Eqs. (46)–(50).

It should be noted that during experimental results, the slope of the saturation functions is assumed to be 0.1 as shown in Fig. 3. Clearly, the reduction of the function slope improves behaviour of the proposed

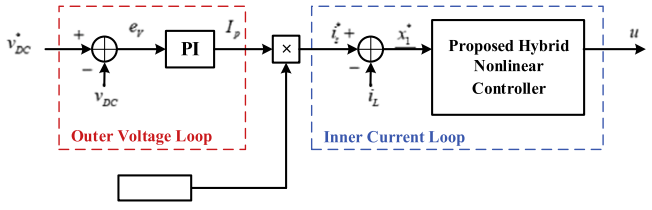

Fig. 2. Developed controller. (For interpretation of the references to color in this figure legend, the reader is referred to the web version of this article.)

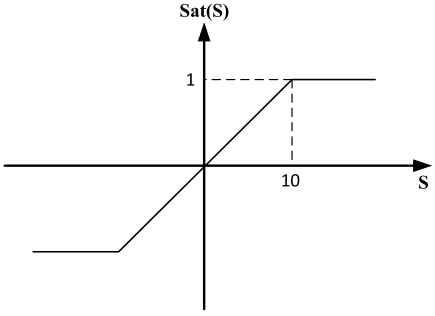

Fig. 3. Employed saturation function for the implementation of the developed controller. (For interpretation of the references to color in this figure legend, the reader is referred to the web version of this article.)

Table 1
Nominal values of the system

Symbol	Parameter	Value	Symbol	Parameter	Value
f_s	grid Frequency	50 *Hz*	f_{sw}	Switching Frequency	20 *kHz*
v_s	grid Voltage	220 v_{rms}	T_s	Sampling time	25 μs
R_S	Nonlinear Load - Series Resistor	2 Ω	k_1	Controller coefficient	8.9×10^5
R_O	Nonlinear Load - Output Resistor	30 Ω	k_2	Controller coefficient	8.9×10^3
C_O	Nonlinear Load - Output Capacitor	100 μF	k_3	Controller coefficient	1.4×10^4
L_1	LCL Filter - Inductor	0.4 *mH*	k_4	Controller coefficient	3
r_{L_1}	LCL Filter – L_1 Equivalent Series Resistance	0.4 Ω	c_1, c_2, c_3	Controller coefficient	1
L_2	LCL Filter - Inductor	1.2 *mH*	K_P	Controller coefficient	0.5
r_{L_2}	LCL Filter - Inductor Series Resistor	1 Ω	K_I	Controller coefficient	7
C	LCL Filter - Capacitor	50 μF	γ_{ii}	Controller coefficient	10^{-9}
C_{dc}	DC Link Capacitor	500 μF			

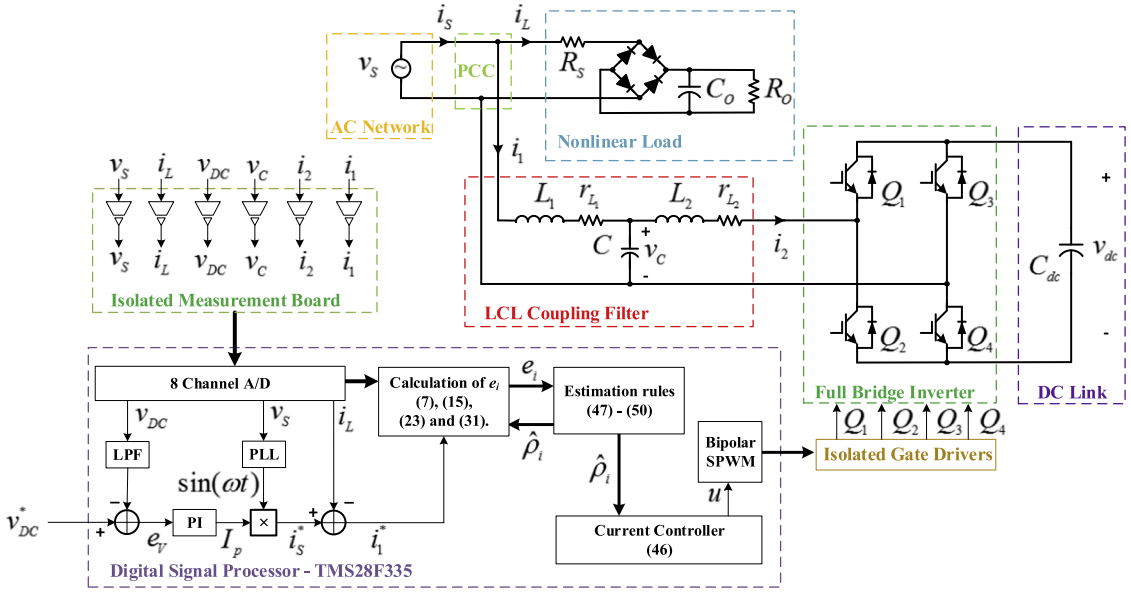

(a)

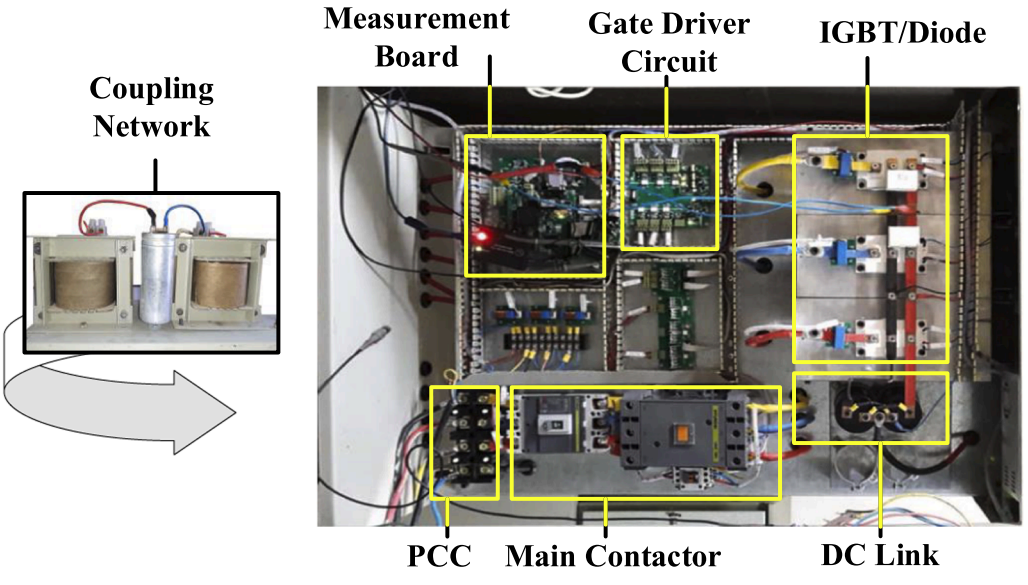

(b)

Fig. 4. Implementation of hybrid nonlinear control of the shunt active power filter with LCL coupling (a) block diagram of the implemented system (b) Practical setup. (For interpretation of the references to color in this figure legend, the reader is referred to the web version of this article.)

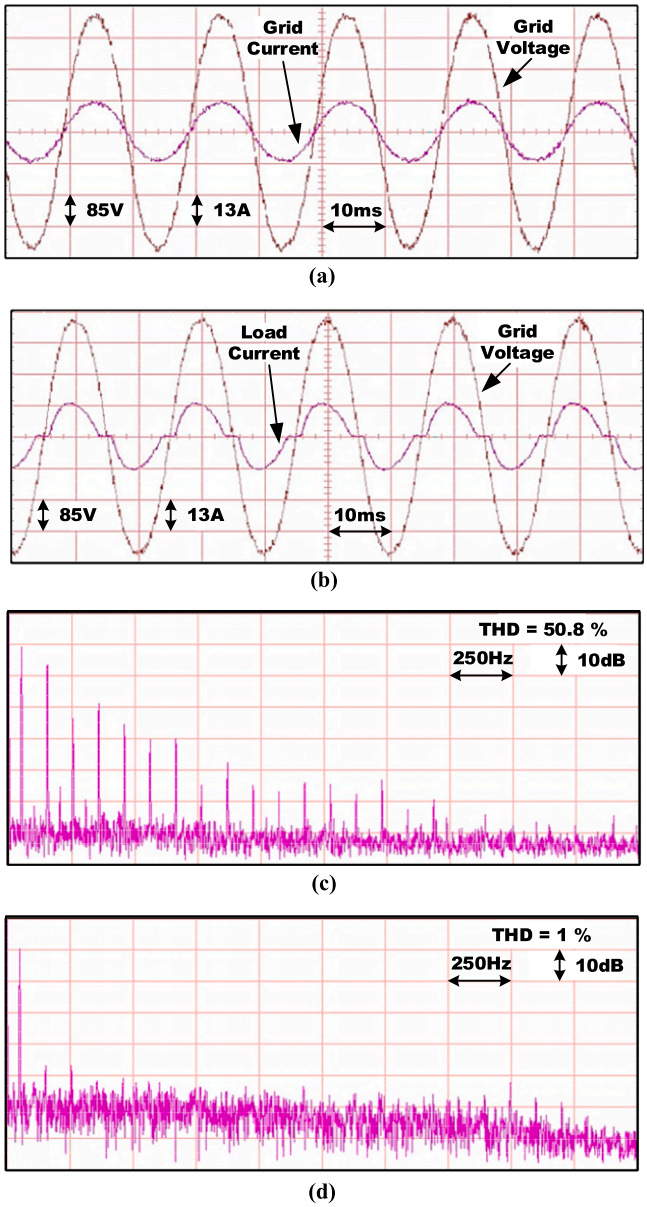

Fig. 5. (a) grid voltage (v_s) and grid current, (b) grid voltage (v_s) and nonlinear load current (i_L) (c) nonlinear load current harmonics (d) harmonics of grid current (i_s). (For interpretation of the references to color in this figure legend, the reader is referred to the web version of this article.)

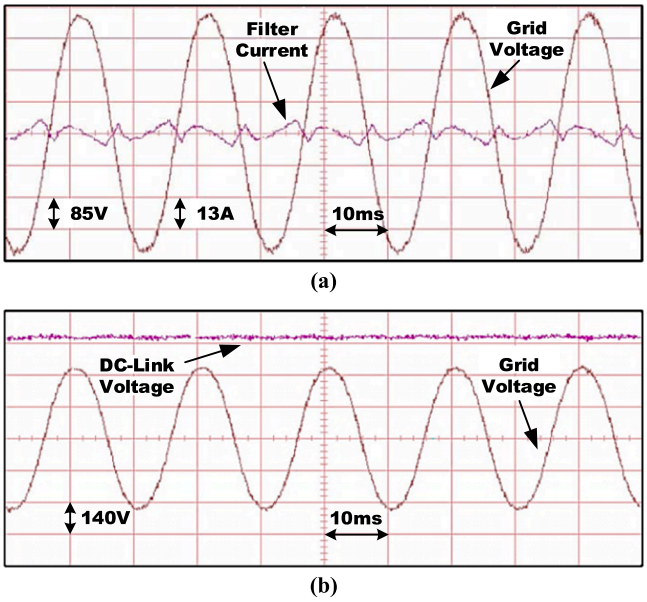

Fig. 6. State variables of SAPF during steady state operation (a) waveform of Grid Voltage (v_s) and filter current (i_1) (b) Waveform of grid current (i_s) and DC-Link voltage (v_{DC}).

controller by reduction of the chattering.

The nominal values of the system are listed in Table 1, and the block diagram of the controller and experimental setup are shown in Fig. 4. Also, to investigate the response of the developed controller, a full-bridge rectifier with RC load is used as a nonlinear load, and the nominal values of load parameters are represented in Fig. 4. The developed controller is implemented using the Texas instruments digital signal processor (DSP-TMS28F335) from Texas instruments.

4.1. First test: steady state response

The grid voltage waveform (v_s), nonlinear load current (i_L), as well as the harmonic spectrum of load current in steady state conditions, are shown in Fig. 5. As it can be seen, the THD of load current is about 50.8%. The developed controller along with the estimation rules are employed for the closed-loop controller of the LCL-type SAPF and then, within the steady-state operation, the grid voltage, filter current, grid current (i_s), DC link voltage (v_{DC}) and harmonic spectrum of both load and grid currents in the presence of the developed controller are illustrated in Fig. 6. It can be seen that the proposed adaptive nonlinear controller can stabilize the closed-loop system and the grid current will be sinusoidal and in phase with the grid voltage after compensation. It should be noted that by using the developed hybrid backstepping controller, the THD of grid current will be about 1%, which is fully compatible with IEEE standards [1]. Moreover, the THD of the developed hybrid nonlinear controller is about 1% better (less) than previous studies: Adaptive PI Controller (2.3650%) [20], Robust Model Reference

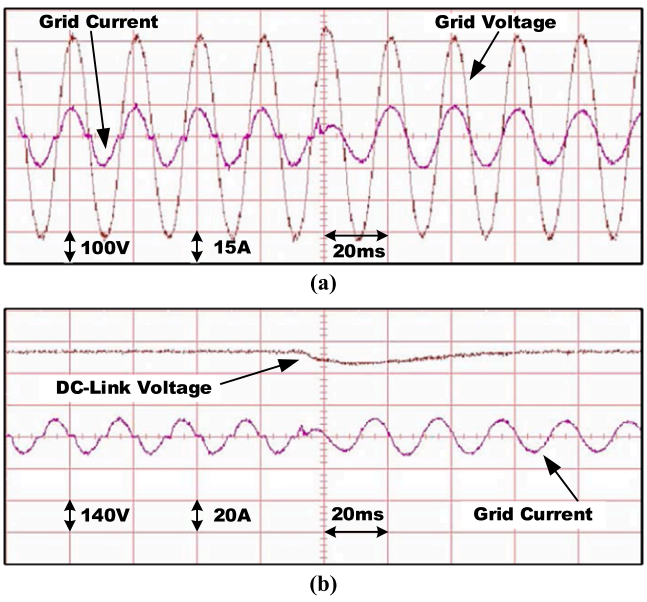

Fig. 7. (a) grid voltage (v_s) and grid current (i_s) during startup of the filter, (b) DC-Link voltage (v_{DC}) and grid current (i_s) at startup. (For interpretation of the references to color in this figure legend, the reader is referred to the web version of this article.)

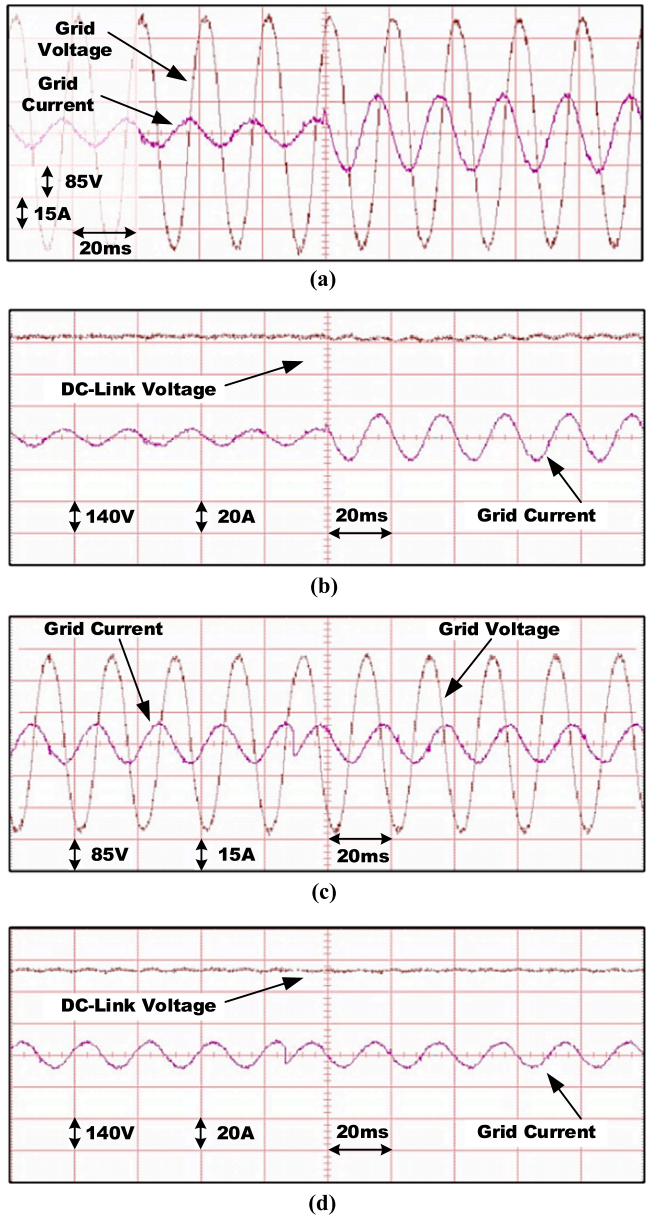

Fig. 8. (a) grid voltage (v_s) and filter current (i_1) during virtual current changing (b) DC-link voltage (v_{DC}) and filter current (i_1) during step change of virtual current magnitude, (c) grid voltage (v_s) and filter current (i_1) during phase change of the virtual current, (d) DC-link voltage (v_{DC}) and filter current (i_1) during phase change of the virtual current. (For interpretation of the references to color in this figure legend, the reader is referred to the web version of this article.)

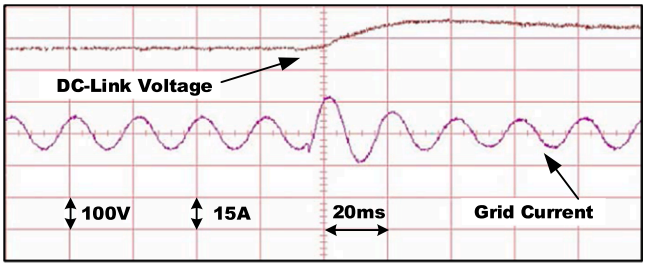

Fig. 9. DC-Link voltage (v_{DC}) and grid current (i_s) during step changing of the DC link voltage. (For interpretation of the references to color in this figure legend, the reader is referred to the web version of this article.)

Adaptive Controller (3%) [16] and Observer-Based Second-Order Sliding Mode Control (1.53%) [18]. Hence, it can be concluded that the proposed hybrid adaptive-nonlinear controller enjoys a superior performance than the conventional backstepping controller in terms of grid current THD.

4.2. Second test: dynamic response of the inner loop

A) *Response of the Controller at Startup*: In this test, to study the dynamic response of the inner loop, the load current feedback is removed at first to make the load current feedback zero. In this condition, the external loop will continue stabilizing the DC link voltage at the reference value (370 V) Then with the steady-state operation of the external loop, the load current feedback is fully applied to the controller. So, the inner loop will start to compensate for the nonlinear load and the dynamic response of the inner load can be recorded. In this test, the grid voltage (v_s), grid current (i_s) and DC link voltage (v_{DC}) are presented in Fig. 7 for investigation of the inner loop dynamic response. Despite significant changes in the load current feedback, the developed hybrid backstepping controller can compensate fully for the local load within a grid cycle. According to Fig. 7b, it is seen that the steady-state error of the DC link voltage is zero despite the changes in inverter output current during the system start-up.

B) *Step changes in the reference current:* To test the dynamic response of the internal loop during step changes of the reference signal, the load current feedback is replaced by a virtual sinusoidal reference signal within the controller and the dynamic response of the controller for a step change in the magnitude of the reference signal is shown in Fig. 8-a and b.

Moreover, for further investigations of the inner loop, the dynamic response of the proposed controller to step changes in the phase angle of the virtual reference signal is demonstrated in Fig. 8-c, d. So, the operating mode of the SAPF will switch from a capacitive leading current to an inductive lagging one (pure reactive reference currents).

Despite having large changes in both the magnitude and phase of the reference current signal, it is observed that the developed controller is quite stable and robust with a very fast dynamic response. It should be noted that within this test, the external loop controller continues stabilizing the DC link voltage without any changes.

4.3. Third test: dynamic response of the external voltage loop

To evaluate the dynamic response of the outer loop, it is assumed that the DC-link reference voltage has been stepped up from 370 to 470 Volts. In this experiment, in addition to the DC link voltage (v_{DC}), the filter current (i_1) is shown as well in Fig. 9. It can be seen, the developed voltage controller can stably track the reference signal satisfactorily with zero steady-state error, despite having a significant change in the reference signal.

5. Conclusion

To benefit from the advantages of backstepping, adaptive, and sliding-mode controllers all at the same time, a hybrid nonlinear approach for closed-loop stabilization of the LCL-type SAPF is developed using Lyapunov stability criteria and asymptotic stability and robustness of the proposed controller is proved analytically within a large range of changes. In addition to the control effort, some estimation rules are developed which will improve the performance of the controller against model uncertainties. By using the TMS320F28335 digital signal processor from Texas Instruments, the experimental response of the designed LCL-type SAPF is investigated and the effectiveness of the designed hybrid controller has been proved in both steady-state and dynamic situations. Despite using a local load with a very high current THD value (about 51%), the developed controller is capable of maintaining the grid current THD within the standard range (around 1%). Moreover, it is shown that the THD improvement of the proposed controller is more efficient than the previous studies. Moreover, considering the experimental results, it is observed that the steady-state error of the proposed nonlinear controller is zero in a wide range of operations.

Declaration of Competing Interest

The authors declare that they have no known competing financial interests or personal relationships that could have appeared to influence the work reported in this paper.

References

[1] "IEEE Recommended Practice and Requirements for Harmonic Control in Electric Power Systems," *IEEE Std 519-2014 (Revision of IEEE Std 519-1992),* pp. 1-29, 2014, doi: 10.1109/IEEESTD.2014.6826459.
[2] A.R. Lubis, M.D. Solihin, M. Affandi, S. Sriadhi, Comparison of Passive LC and Passive Single Tuned Filters in Reducing Current Harmonics, EAI, 2019, https://doi.org/10.4108/eai.18-7-2019.2288603, 2019-11-26.
[3] M.A.A.M. Zainuri, M.A.M. Radzi, A.C. Soh, N. Mariun, N.A. Rahim, DC-link capacitor voltage control for single-phase shunt active power filter with step size error cancellation in self-charging algorithm, IET Power Electron. 9 (2) (2016) 323–335, https://doi.org/10.1049/iet-pel.2015.0188.
[4] M.T. Bina, A new complementary method to instantaneous inactive power compensation, in: IEEE 34th Annual Conference on Power Electronics Specialist, 2003. PESC '03 4, 2003, pp. 1542–1547, https://doi.org/10.1109/PESC.2003.1217688, 15-19 June 2003vol. 4.
[5] J. Zhou, Y. Yuan, H. Dong, Adaptive DC-link voltage control for shunt active power filters based on model predictive control, IEEE Access 8 (2020) 208348–208357, https://doi.org/10.1109/ACCESS.2020.3038459.
[6] G. Goswami, P.K. Goswami, Power quality improvement at nonlinear loads using transformer-less shunt active power filter with adaptive neural fuzzy interface system supervised PID controllers, Int. Trans. Electr. Energy Syst. 30 (7) (2020) e12415, https://doi.org/10.1002/2050-7038.12415.
[7] L. Yang, J. Yang, A robust dual-loop current control method with a delay-compensation control link for LCL-type shunt active power filters, IEEE Trans. Power Electron. 34 (7) (2019) 6183–6199, https://doi.org/10.1109/TPEL.2018.2865813.
[8] T. Gao, Y. Lin, D. Chen, L. Xiao, A novel active damping control based on grid-side current feedback for LCL-filter active power filter, Energy Rep. 6 (2020) 1318–1324, https://doi.org/10.1016/j.egyr.2020.11.027, 2020/12/01/.
[9] L. Yang, J. Yang, M. Gao, A. Watson, P. Wheeler, Current control of LCL-type shunt APFs: damping characteristics, stability analysis, and robust design against grid impedance variation, IEEE J. Emerg. Select. Topics Power Electron. 9 (4) (2021) 5026–5042, https://doi.org/10.1109/JESTPE.2020.3017551.
[10] S. Eren, M. Pahlevaninezhad, A. Bakhshai, P.K. Jain, Composite nonlinear feedback control and stability analysis of a grid-connected voltage source inverter with LCL filter, IEEE Trans. Ind. Electron. 60 (11) (2013) 5059–5074, https://doi.org/10.1109/TIE.2012.2225399.
[11] R. Bimarta, K.H. Kim, A robust frequency-adaptive current control of a grid-connected inverter based on LMI-LQR under polytopic uncertainties, IEEE Access 8 (2020) 28756–28773, https://doi.org/10.1109/ACCESS.2020.2972028.
[12] J. Li, Y. Zhang, Y. Zhao, L. Ren, J. Wang, Y. Liu, An improved three-stages cascading passivity-based control of grid-connected LCL converter in unbalanced weak grid condition, IEEE Access 9 (2021) 89497–89506, https://doi.org/10.1109/ACCESS.2021.3091210.
[13] J. Khazaei, Z. Tu, A. Asrari, W. Liu, Feedback linearization control of converters with LCL filter for weak AC grid integration, IEEE Trans. Power Syst. 36 (4) (2021) 3740–3750, https://doi.org/10.1109/TPWRS.2021.3049324.

[14] H. Katir, et al., Fault tolerant backstepping control for double-stage grid-connected photovoltaic systems using cascaded H-bridge multilevel inverters, IEEE Control Syst. Lett. 6 (2022) 1406–1411, https://doi.org/10.1109/LCSYS.2021.3095107.
[15] G.V. Hollweg, P.J.D. de Oliveira Evald, R.V. Tambara, H.A. Gründling, A robust adaptive super-twisting sliding mode controller applied on grid-tied power converter with an LCL filter, Control Eng. Pract. 122 (2022), 105104, https://doi.org/10.1016/j.conengprac.2022.105104, 2022/05/01/.
[16] D.M.C. Milbradt, G.V. Hollweg, P.J.D. de Oliveira Evald, W.B. da Silveira, H. A. Gründling, A robust adaptive one sample ahead preview controller for grid-injected currents of a grid-tied power converter with an LCL filter, Int. J. Electr. Power Energy Syst. 142 (2022), 108286, https://doi.org/10.1016/j.ijepes.2022.108286, 2022/11/01/.
[17] R.V. Tambara, J.M. Kanieski, J.R. Massing, M. Stefanello, H.A. Gründling, A discrete-time robust adaptive controller applied to grid-connected converters with LCL filter, J. Control Autom. Electr. Syst. 28 (3) (2017) 371–379, https://doi.org/10.1007/s40313-017-0313-3, 2017/06/01.
[18] B. Guo, et al., Observer-based second-order sliding mode control for grid-connected VSI with LCL-type filter under weak grid, Electr. Power Syst. Res. 183 (2020), 106270, https://doi.org/10.1016/j.epsr.2020.106270, 2020/06/01/.
[19] M. Salimi, J. Soltani, A. Zakipour, Experimental design of the adaptive backstepping control technique for single-phase shunt active power filters, IET Power Electron. 10 (8) (2017) 911–918, https://doi.org/10.1049/iet-pel.2016.0366.
[20] P.J. Dias de Oliveira Evald, G. Vieira Hollweg, R. Varella Tambara, H.A. Gründling, A new discrete-time PI-RMRAC for grid-side currents control of grid-tied three-phase power converter, Int. Trans. Electr. Energy Syst. 31 (10) (2021) e12982, https://doi.org/10.1002/2050-7038.12982.

Vadood Hajbani was born in Iran in 1986. He obtained his B. Sc. and M.Sc. degrees in Electrical Engineering from Islamic Azad University (IAU), Iran, in 2011 and 2014, respectively, from the Ardabil and Ahar branches. Between 2011 and 2017, he worked as a lecturer at the Islamic Azad University (IAU) in Ardabil, Iran. His research interests include the control of switching power converters and power electronics.

Adel Zakipour was born in Ardabil, Iran, in 1981. He received his Ph.D. degrees in Electrical Engineering from K.N.Toosi University of technology, Tehran, Iran, in 2017. Currently, he is an assistant professor in power electronics at department of electrical engineering, Arak university of technology. His research interests include design and control of the DC/DC and DC/AC converter, grid connected inverters and variable speed drive.

Mahdi Salimi (corresponding author) graduated in electrical engineering from Islamic Azad University (IAU) (Science and Research Branch), Tehran, Iran, in 2012. He worked as an Assistant Professor from 2012 until 2019 at the IAU University, Ardabil Branch, Iran, in the Electrical and Electronics Department. In 2019 he joined the University of Nottingham, Power Electronics, Machine, and Control (PEMC) Group as a Researcher for three years. Since April 2022, he has worked at Greenwich University as a Lecturer of power electronics. He has published 36 papers in peer-reviewed journals with 24 papers published in international conferences. His research areas include design, closed-loop control, simulation, and practical implementation of the power electronics systems for more or full electric aircraft and vehicles, grid-connected renewable energy systems, and active power filters.